



# Efficiency of Ozone Production in Coplanar Dielectric Barrier Discharge

T. Homola<sup>1</sup> · B. Pongráč<sup>2</sup> · M. Zemánek<sup>1</sup> · M. Šimek<sup>2</sup>

Received: 19 February 2019 / Accepted: 9 April 2019 / Published online: 27 April 2019  
© Springer Science+Business Media, LLC, part of Springer Nature 2019

## Abstract

Efficient generation of ozone by cold atmospheric plasmas is interesting for sterilisation and decontamination of thermally-sensitive surfaces. This paper presents a study of robust coplanar dielectric barrier discharge (DBD) for generating atmospheric pressure plasma in synthetic air and in oxygen. The atmospheric plasma generated by coplanar DBD in synthetic air showed considerably high ozone production of 2.41 g/h (2.25 slm, 45 W), while the production yield and energy cost were 54 g/kWh and 40.9 eV/molecule. The use of oxygen instead of synthetic air, at much lower discharge power (2.25 slm, 17 W), maintained the ozone production of 2.35 g/h, whereas the production yield significantly increased to 138 g/kWh with a corresponding energy cost of 12.9 eV/molecule. The temperature of coplanar DBD ceramics in synthetic air (45 W) and oxygen (17 W) plasma generation (continuous alternating-current operation) showed temperatures below 70 °C and 30 °C, respectively. The rotational temperatures obtained from optical emission spectroscopy indicated similar gas temperatures in the thin plasma layer close to the surface of the DBD ceramics. The low temperature of the plasma–ceramics interface evidences the applicability of coplanar DBD for the contact treatment of thermally sensitive surfaces where a high concentration of ozone is required.

**Keywords** Ozone generation · Dielectric barrier discharge · Cold plasma · Coplanar DBD · Low-temperature plasma

## Introduction

Dielectric barrier discharge (DBD) is considered to be the most efficient method for ozone generation among electrical plasma generators [1]. DBDs are usually generated using high-voltage (HV) alternating-current (AC) sources connected to two metallic

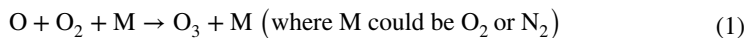
---

✉ T. Homola  
tomas.homola@mail.muni.cz

<sup>1</sup> R&D Center for Low-Cost Plasma and Nanotechnology Surface Modifications (CEPLANT), Department of Physical Electronics, Faculty of Science, Masaryk University, Kotlářská 267/2, 611 37 Brno, Czech Republic

<sup>2</sup> Department of Pulse Plasma Systems, Institute of Plasma Physics v.v.i, Czech Academy of Sciences, Za Slovankou 3, 182 00 Prague, Czech Republic

electrodes which are separated by thin layers of a dielectric material placed in the space between them. Typical materials to create dielectric barriers in DBDs are glass, quartz, ceramics, and polymers. The dielectric material collects charged species generated by the discharge, which creates an electrical field with inverse electrical intensity. This inevitably leads to suppression of the external electrical field and, consequently, causes the extinction of electrical discharge, which lasts for some tens of nanoseconds and has a typical radial dimension of filaments on the order of tens to hundreds of micrometres [2, 3]. Such events are therefore called micro-discharges, and their lifetimes are shorter than the time required for thermalisation of plasma, which gives DBD plasma its low-temperature, non-equilibrium attributes. Since the stability of the ozone ( $O_3$ ) molecule is very sensitive to the temperature of the gas,  $T_g$ , it is crucial to keep the  $T_g$  in the discharge zone as low as possible in order to maintain reasonable ozone production yield. A concentration of ozone generated through plasma-assisted  $O_2$  dissociation represents a dynamic balance between processes of ozone formation and destruction [4]. Ozone is mainly formed by three-body collisions, in which an oxygen atom and an oxygen molecule must collide together with the third particle. It is obvious that this type of reaction is more efficient for electrical discharges at atmospheric pressure because three body collisions are of low probability at low pressures.



The most important reactions leading to decomposition of ozone are:



The rate constants of reactions (3)–(8) increase exponentially with increase of  $T_g$ .

The application of various DBDs for ozone generation is widespread since its invention by Siemens in 1857 [5]. The construction and design of DBDs have been continuously improved, and, according to the geometry used, we classify three basic types of DBDs: volume [6], surface [7, 8], and coplanar DBD [9]. Also, hybrid systems have been reported [10]. Nassour et al. [1] compared ozone generation efficiency between volume and surface DBDs. It was found that the energy efficiency of a surface DBD was approximately three times higher than that of a volume DBD. Šimek et al. [11] investigated the influence of power modulation on  $O_3$  production in a surface DBD. The highest energy efficiency for ozone production was obtained by combining a low duty cycle with a suitable AC high-voltage amplitude, which led to the production of micro-discharges distributed homogeneously over the surface DBD electrode system. Recently, the amplitude-modulation of the driving AC high voltage has also been tested in connection with the traditional coaxial cylindrical DBD to develop a unique, practical ozone generator with widely adjustable ozone concentration and nearly constant ozone yield, simultaneously [12].

An apparent drawback of the surface DBD consists in the exposure of the powered metallic electrode to plasma and consequent erosion due to the bombardment of the electrode by energetic particles from plasma. This limits the lifetime of the surface DBD to hundreds of hours [13]. The coplanar DBD geometry has an entire electrode system embedded in dielectric material, and plasma, therefore, does not come into contact with metallic surfaces, which significantly increases its lifetime. The coplanar DBD plasma for surface treatments of various materials at atmospheric pressure has been reported by Černák et al. [14], Skácelová et al. [15, 16], Medvecká et al. [17, 18], Prysiazhnyi et al. [19], Krumpolec et al. [20], and Homola et al. [21, 22]. All of them used a variety of coplanar DBD called ‘diffuse coplanar surface barrier discharge’, which consists of a coplanar electrode system printed on alumina dielectric, partially immersed in a high-quality insulating fluid. The insulating fluid serves here to remove an excess of produced heat and keeps the intensity of the electric field around printed coplanar electrodes as low as possible. Because of low electrical intensity around the coplanar electrodes, the micro-discharges are generated on the other side of the alumina ceramics, which is exposed to the working gas (ambient air or various technical gases). The insulating fluids such as mineral and synthetic oils provide sufficient electrical and thermal insulation at higher temperatures, which are typically around 70 °C [23]. Such an arrangement seems to be appropriate for surface treatments; however, the overall temperature of the ceramic surface is still high, which should be considered if the generation of ozone or treatment of heat-sensitive materials is envisaged.

Furthermore, recent progress in applied plasma physics [24] has brought into attention plasma agriculture—an emerging field of plasma application for enhancement of plant seeds’ growth via direct/indirect treatment of their surfaces by transient or reactive species, such as atomic oxygen, ozone (O<sub>3</sub>), and other reactive species, produced by micro-discharges [25–30]. Ozone is of particular importance because it can be produced in large quantities and serves as a decontamination agent against various pathogens present on the surface of seeds [31–33].

The direct treatment of seeds by the dielectric barrier discharges requires close contact of thermally sensitive seeds with DBD dielectric surfaces. Therefore, the motivation of this work was to establish the relation between the temperature of the dielectric surface of coplanar DBD during typical continuous AC operation and its impact on ozone generation. A novel DBD concept consisting of coplanar electrodes fully embedded in alumina ceramic without the need for any cooling liquid was employed in this study.

## Experimental

The experimental setup is schematically shown in Fig. 1. It consists of the coplanar dielectric barrier discharge electrode system power supply; heatsink and fan cooling unit; gas feeding with mass flow controller; ozone, NO<sub>2</sub> and N<sub>2</sub>O analysers; and ICCD-based emission spectrometer.

### Coplanar Dielectric Barrier Discharge

The surface plasma for ozone production was generated using coplanar dielectric barrier discharge in synthetic air (99.999%; containing H<sub>2</sub>O < 2 ppm, CO + CO<sub>2</sub> < 0.4 ppm) and oxygen (99.999%; containing N<sub>2</sub> < 5 ppm, H<sub>2</sub>O < 2 ppm, CO + CO<sub>2</sub> < 0.4 ppm). In total, 50 coplanar electrodes were embedded in 1.15 mm thick alumina ceramic. Both line width

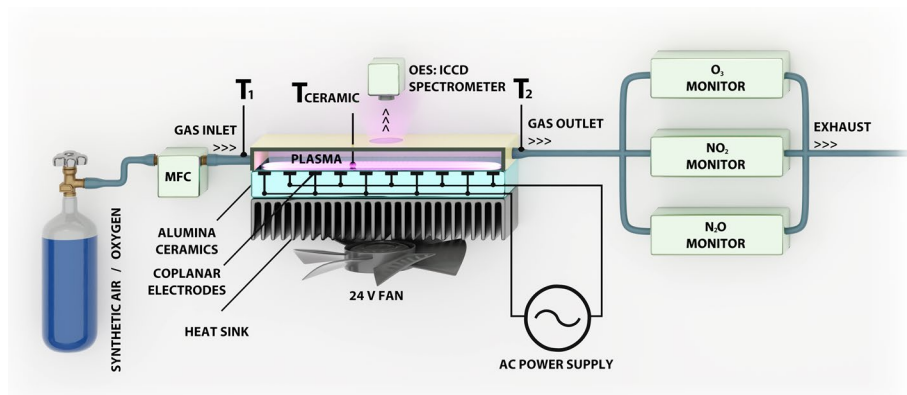


**Fig. 1** Schematic diagram of the experimental set-up

of the electrode strip and the gap between the adjacent strips were 0.5 mm. The thickness of alumina ceramic above coplanar electrodes was 0.15 mm. The total size of the active plasma area was approx. 25 cm<sup>2</sup>. The coplanar ceramics was manufactured by Kyocera, Japan. A compact coplanar DBD electrode design without insulating fluids used in this work provides higher versatility and better possibilities for cooling using either passive or active elements. In this work, the coplanar ceramic electrode system was attached to the metallic heatsink using standard thermal paste and further cooled with a 24 V fan (consuming approx. 1.5 W). The passive cooling of the coplanar electrode system in conjunction with the flow of the working gas led to lower ceramic temperatures, which decreased from approx. 70 °C to approx. 50 °C.

The coplanar DBD was powered by continuous-wave sinusoidal AC high voltage with the frequency of approx. 19 kHz. The total power input was monitored by an OM 402PWR wattmeter and Rigol DS1104 Z-S Plus oscilloscope. Total power input was 55 W for synthetic air and 27 W for oxygen. The energy loss in the HV power source, including thermal losses in the transformer, was approximately 10 W; therefore, power in the plasma was approx. 45 W for synthetic air and approx. 17 W for oxygen. The power density for air and for oxygen was 2.2 W/cm<sup>2</sup> and 1.1 W/cm<sup>2</sup>, respectively. The pressure in the reactor was monitored by TPG 260 piezo gauge (Pfeifer Vacuum) and always kept at 1 atm (760 Torr). The flow of the working gas was directed along the ceramic surface perpendicularly with respect to the coplanar electrode-strips. A Bronkhorst HI-TEC mass-flow controller was employed to monitor the volume of working gas flowing through the system, in standard litres per minute (slm).

### **O<sub>3</sub>, NO<sub>2</sub> and N<sub>2</sub>O Measurement**

We studied the formation of O<sub>3</sub>, NO<sub>2</sub>, and N<sub>2</sub>O generated by coplanar DBD in synthetic air and oxygen at various gas flows ranging from 2 to 10 slm. The concentrations of the discharge products were monitored outside the discharge chamber. A Teflon tube was used for sampling the products. Concentrations of O<sub>3</sub>, N<sub>2</sub>O, and NO/NO<sub>2</sub> were determined by means of non-dispersive UV absorption ozone monitor Model 465 M, infrared N<sub>2</sub>O analyser API 320E, and chemiluminescence NO<sub>x</sub> analyser model 200EM (all Teledyne

Instruments), respectively. The minimum fed flow of 1 slm was due to minimal consumption of ozone, nitrous oxide, and nitrogen dioxide by the measurement devices.

The length of the Teflon tube between the reactor outlet and the gas analysers was approx. 1.5 m; therefore, potential ozone losses due to interaction with the surface of the tube are of concern, especially when efficiency of ozone production (i.e., production yield and energy cost) need to be determined. To evaluate losses during transport of the discharge products to the Model 465 M analyser, we performed a simple test with both air and pure oxygen using a stabilised Hg lamp (a source of UV photons) closed inside a small Pyrex cylinder flushed (1 slm) with either synthetic air or pure oxygen. UV radiation photo-dissociates oxygen molecules, producing ozone. At the exit of the Pyrex cylinder, we measured (with the cylinder connected to the Model 465 M using a Teflon tube of minimal length  $D_0=0.1$  m) stable concentrations of 60 ppm and 180 ppm of ozone in air and oxygen, respectively. Then, the length of the Teflon tube was changed from minimal length  $D_0$  to  $D_0+l$ , where  $l=0.125$  m, 0.25 m, 0.5 m, 1 m, and 2 m, and we found that the concentration of ozone was almost identical, i.e., within the  $\pm 2\%$  fluctuation around the average. This conclusion is valid for the lowest flow rate of 1 slm, i.e., for the highest residence/transit time. For higher flow rates (lower transit times) and higher ozone concentrations, the influence of the tube length should be lower, i.e., negligible. We concluded that the effect of the tube length between 0.15 and 3 m on the measured concentration of the ozone was negligible and within experimental error (caused by the discharge fluctuations, temperature drifts, etc.) for ozone concentrations  $> 500$  ppm.

## Optical Emission Spectroscopy (OES)

The vibrational distributions and rotational temperatures in plasma were calculated from optical emission spectra acquired via an optical fibre connected to the iHR320 ICCD spectrometer. The plasma-induced emission generated by micro-discharges on the ceramic surface was collected and projected onto the entrance slit of the spectrometer. Emission spectra were elaborated by using an approach described in detail in [34]. Vibrational distributions and rotational temperatures (assuming Boltzmann population of rotational levels of vibronic states) of emission bands were determined after approximating the instrumental function of the iHR320 by assuming a triangular shape for the grating used and using the known entrance slit width.

## Results and Discussion

### Electrical and Thermal Characteristics

The experimental current and voltage (I–V) waveforms of coplanar DBD plasma appear in Fig. 2. The real power in the plasma was calculated by integrating current and voltage ( $P = \int (I \cdot U) dt$ ). Figure 2a shows I–V waveforms of synthetic air plasma and Fig. 2b shows the I–V waveforms of oxygen plasma. The total consumed power was 55 W and 27 W for synthetic air and oxygen, respectively. The discharge power delivered to plasma was found to be 45 W and 17 W, respectively. The difference of 10 W between the total consumed power and discharge power was due to the electrical losses in the power supply and transformer.

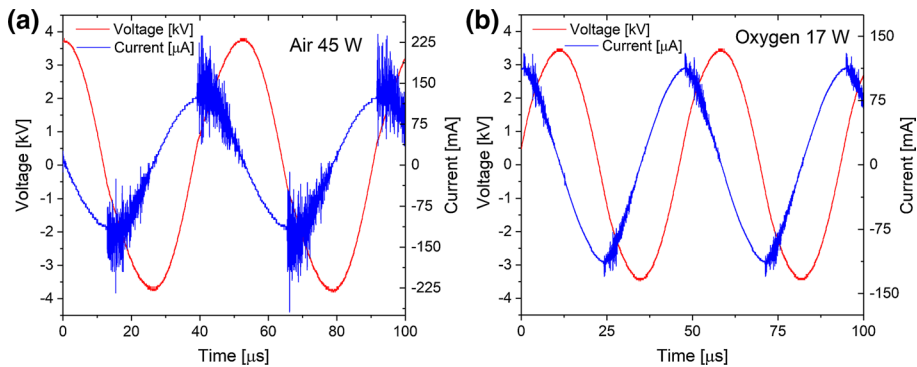


**Fig. 2** Experimental I–V waveforms for coplanar DBD generated in **a** synthetic air at a discharge power of 45 W and **b** in oxygen at a discharge power of 17 W

The efficiency of ozone generation obtained by using a similar coplanar DBD manufactured by Kyocera has been recently reported by Jōgi et al. [35]. The study reports a different powering setup which uses a signal generator whose output voltage is amplified by an audio amplifier and subsequently is converted to high driving voltage by a transformer. The voltage pattern of the signal generator was a sine wave with a frequency ranging from 100 Hz to 6 kHz (200 Hz to 2 kHz for Fig. 1 in Ref. [35]). This arrangement is suitable for power outputs in the range of tens of watts. However, for more powerful and industrial applications, we present a coplanar DBD powered directly by the voltage supplied from a standard electrical supply. The generator was designed to operate in half or full bridge topology. The signal of the primary winding in the transformer is the alternating voltage of the rectangular shape. Thanks to the scattering inductance present in the HV transformer and the coplanar DBD capacity, which together form a second order filter, the voltage applied to the coplanar DBD results in a sine wave. As a result, we powered the coplanar DBD by a sine wave of approx. 19 kHz. The use of high operating frequencies leads to the lower working voltage on the electrode and longer electrode lifetime.

Jōgi et al. [35] used a Peltier cell and water cooling systems in order to keep the temperature of the gas within the range of 25 °C to 30 °C; unfortunately, temperature of the surface, which is critical for treating biological or other temperature-sensitive materials, was not reported. Furthermore, energy consumed by cooling with the Peltier element (which might be comparable to the power supplied to the discharge) was not included in the calculations of the specific input energy (SIE) value and, consequently, was not included in the estimation of the O radical and O<sub>3</sub> production efficiencies.

The thermal properties of the reactor were determined by precise thermometers placed at (1) gas input, (2) close to the ceramic surface that is in contact with the plasma, and (3) at the gas output. The measured temperatures together with power loss due to the gas flow are displayed in Fig. 3. The input temperature of the synthetic air was, as expected, constant at approx. 22 °C, which was equal to the temperature in the laboratory. The temperature measured above the coplanar DBD ceramic was maximally 70 °C for zero flow of the synthetic air. Increasing the synthetic air flow led to a gradual and nearly linear decrease of the temperature above the ceramic, which was found to be 50 °C for the highest flow of the synthetic air of 10 slm. The temperature of the synthetic air at the output slightly increased with an increase of the air flow.

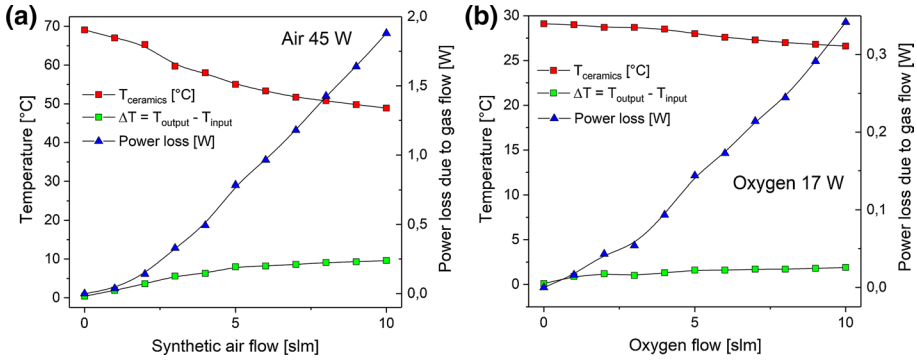


**Fig. 3** Temperature of ceramics, difference between output and input temperatures and power loss due to the gas flow for **a** synthetic air at 45 W and oxygen at 17 W

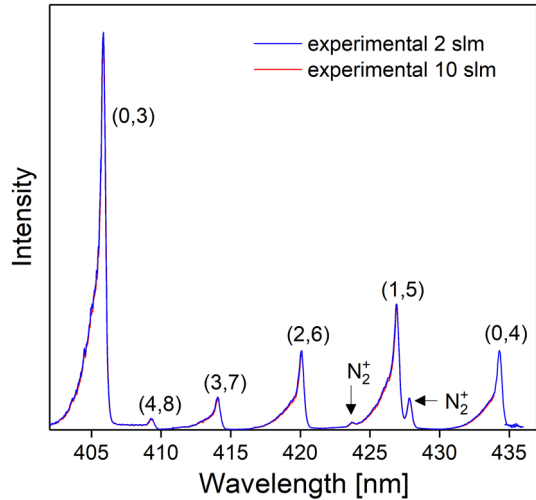
### Optical Emission Spectroscopy

Optical emission spectroscopy (OES) was used to record vibrational and rotational electronic states of a nitrogen molecule in the synthetic air for all used flows ranging from 2 to 10 slm. Concerning the UV emission spectra, strong bands belonging to the second positive system (SPS) of neutral molecular nitrogen  $N_2(C^3\Pi_u \rightarrow B^3\Pi_g)$  as well as weaker bands of the first negative system (FNS) ( $B^2\Sigma_u^+ \rightarrow X^2\Sigma_g^+$ ) of  $N_2^+$  were detected. The intensity of SPS/FNS spectral bands increased with increasing DBD power, and, because the pressure and hence also the density of nitrogen molecules was constant (1 atmosphere). An observed increase of intensities of detected spectral bands was due to an increase of the density of filaments produced during an AC cycle, which roughly doubled as well. The dominant mechanism of the excitation and ionisation of  $N_2$  molecules to the radiative  $N_2(C^3\Pi_u)$  and  $N_2^+(B^2\Sigma_u^+)$  electronic states is the electron impact process occurring at the rate which is strongly linked with the electron energy distribution function (EEDF) [34].

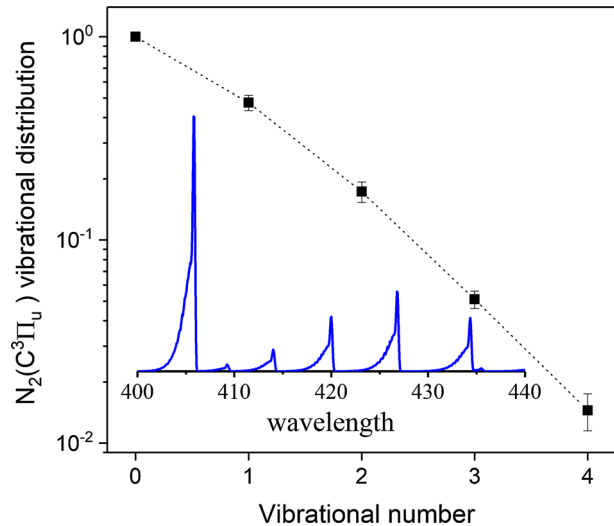
Figure 4 shows comparison of two spectra of the SPS emission for air flows of 2 slm and 10 slm in the 395–435 nm spectral range (containing bands belonging to the  $\Delta v = -3, -4$  sequences). There was no noticeable difference between spectra recorded for the lowest and highest flows. Therefore, characteristic vibrational and rotational temperatures of micro-discharges occurring at the gas–dielectric interface are not strongly influenced by the flow of the gas. Figure 5 shows an example of the vibrational distribution of  $N_2(C^3\Pi_u, v=0-4)$  levels derived from experimental spectra (such as displayed in Fig. 4.) using a technique detailed in [34]. Since the efficiency of ozone production is very sensitive to the temperature of the gas, which is in our case reflected by the rotational temperature of the  $N_2(C^3\Pi_u, v)$  state [36], we determined the rotational temperature by fitting partially-resolved SPS(0,3) and SPS(2,6) bands.

Figure 6a, b show a comparison of experimental and simulated band profiles for the SPS(0,3) and SPS(2,6) bands giving 350 K (~80 °C) and 385 K (~115 °C), respectively. The difference in the rotational temperature is within the standard error of approx.  $\pm 30$  K, which was reported also in other works [10, 37]. The temperature of gas for plasma generated in synthetic air (45 W, 2 slm) is clearly in within the range 80–115 °C, which correlates well with the temperature measured above the ceramic presented in Fig. 3a. The temperature measured directly above the ceramic was approx. 65 °C, slightly lower than the temperature calculated from OES measurement.

**Fig. 4** Characteristic optical emission of  $N_2(C^3\Pi_u)$  electronic state in the 395–435 nm spectral range acquired from discharge in synthetic air for mass flows of 2 slm and 10 slm



**Fig. 5** Characteristic vibrational distribution of the  $N_2(C^3\Pi_u, v=0-4)$  electronic state obtained by fitting experimental spectra shown in Fig. 4. The inset in the figure shows a corresponding synthetic spectrum of the SPS emission produced for  $T_{rot}=350$  K and calculated according to the model described in [34]



## Production of Ozone, Nitrous Oxide, and Nitrogen Dioxide

Figure 7 shows ozone ( $O_3$ ) and nitrous oxide ( $N_2O$ ) concentrations generated by coplanar DBD plasma in synthetic air at various flows ranging from 1 to 10 slm. At the minimal flow of synthetic air at 1 slm, the concentration of ozone was 2987 ppm and increased to 3690 ppm for synthetic air flow at 2.25 slm. 3690 ppm was the maximal measured concentration, and a further increase of synthetic air flow led to decrease of concentration to 1878 ppm for the flow of 10 slm. The initial increase in ozone concentration is clearly related to the need for a higher volume of working gas until saturation is reached. Then, a decrease of ozone concentration with the increasing flow is caused by progressive dilution of ozone and increasing self-cooling of the discharge surface (Fig. 3a).

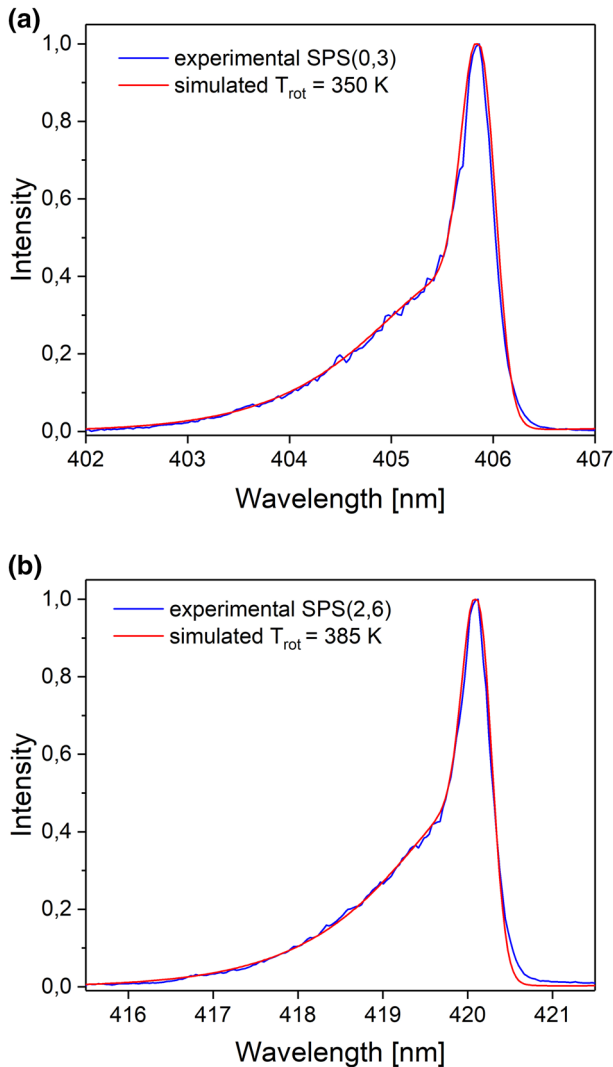
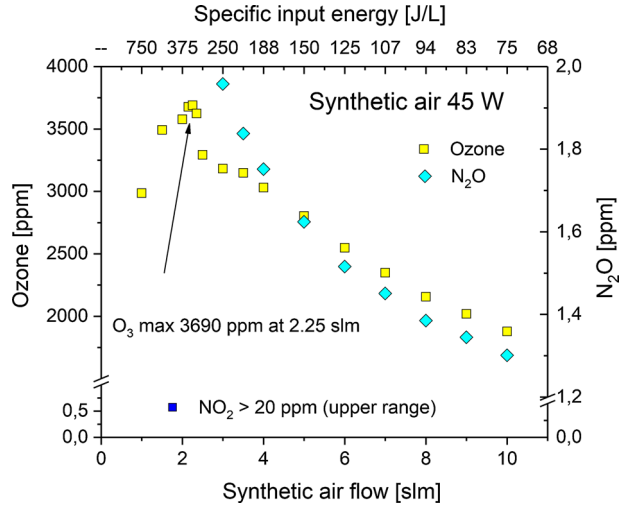


**Fig. 6** Experimental and simulated spectra used for  $T_{rot}$  determination for **a** SPS(0,3) and **b** SPS(2,6). Experimental spectra acquired in synthetic air at discharge power of 45 W and flow of 2 slm

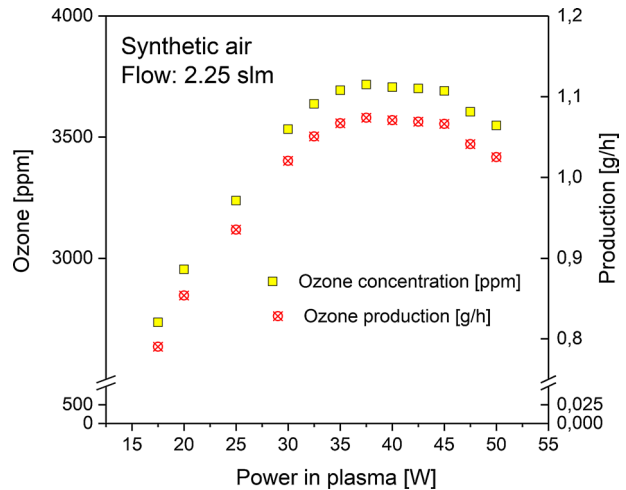
The concentration of nitrous oxide ( $N_2O$ ) was found at approximately 2 ppm for synthetic air flow 3 slm. Since the  $O_3/N_2O/NO_x$  measuring devices consumed around 2 slm, continuous measurement of all monitored compounds at the same time was possible only at minimal flow 3 slm. The concentration of  $N_2O$  decreased with increase in synthetic air flow and reached 1.3 ppm for flow 10 slm. Production of nitrogen dioxide ( $NO_2$ ) was always higher than 20 ppm and out of range of the  $NO_2$  analyser.

Figure 8 shows the concentration of ozone as a function of power in plasma. The flow was kept constant at 2.25 slm, which was the most efficient flow of synthetic air (in current geometry) to reach a maximal concentration of ozone.

**Fig. 7** O<sub>3</sub> and N<sub>2</sub>O concentration [ppm] in synthetic air at various flows



**Fig. 8** O<sub>3</sub> concentration in synthetic air with flow of 2.25 slm at various discharge powers ranging between 15 and 50 W



The coplanar plasma operated at 17 W showed ceramic surface non-homogeneously covered by plasma with distinguishable–recognised micro-discharges. An increase in power led to an increase in the number of micro-discharges and subsequently to an increase in the inhomogeneities in plasma. The plasma appeared homogeneous and visually diffuse at power of approximately 40–45 W. The concentration of ozone at minimal power 17 W was approx. 2700 ppm and linearly increased with power to 3693 ppm for power 35 W. Further increase of ozone concentration as a function of power in the range between 35 and 45 W was negligible. The change in the power between 35 and 45 W changed the plasma only visually; the plasma-induced emission was more intense and visually more diffuse. Ozone concentration decreased for power higher than 45 W. The decrease in ozone concentration for power > 45 W was because of thermal decomposition of ozone due to increased temperature of the ceramics.

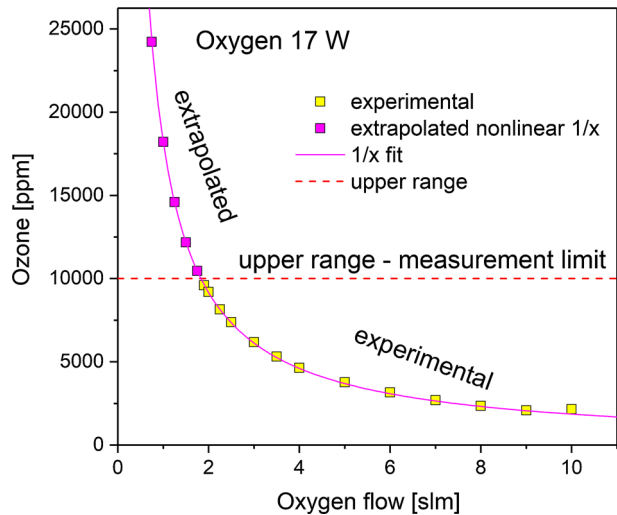
Figure 9 presents the concentration of ozone generated in oxygen at various flows ranging from 1.9 to 10 slm. Figure 9 shows both experimental and extrapolated data because flows of oxygen lower than 1.9 slm led to ozone concentrations higher than 10,000 ppm, which was the limit of the ozone monitor system and out of its linear range. The total power in the plasma was 17 W, which is less than half of the power used in the measurements of ozone in synthetic air presented in Fig. 7.

Considering the results presented in Figs. 7 and 8, using the same power of 17 W, the concentration of ozone in air and oxygen at the same flow was approx. 2700 and 10,000 ppm, respectively, which is almost a 300% increase. In contrast to synthetic air, the decrease of ozone concentration with increase of oxygen flow was not linear. The significant difference in O<sub>3</sub> production between synthetic air and oxygen feed gases has multiple reasons. For instance, the significance of a higher amount of oxygen, which is an essential precursor for O<sub>3</sub> production, is straightforward. On the other hand, reactions in synthetic air generate atomic nitrogen N(<sup>4</sup>S, <sup>2</sup>D, <sup>2</sup>P) which is further converted to nitric oxide through (6), followed by a chain of reactions that reduce the quantity of both oxygen and ozone species [4].

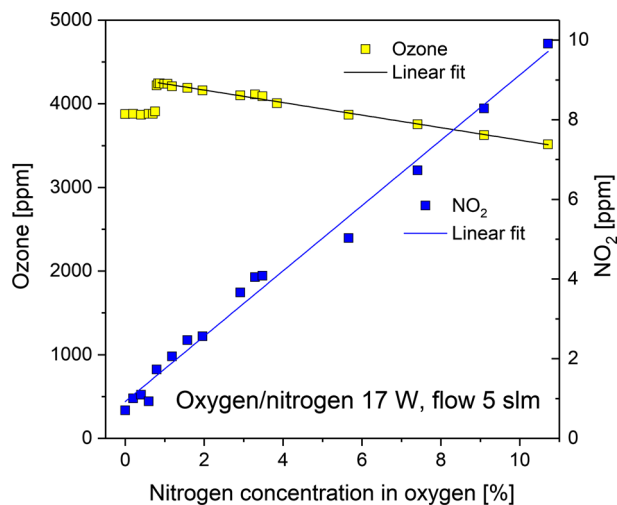
Figure 9 also shows extrapolated results for flows lower than 1.9 slm. However, the calculation of saturation flow, in this case, is not very clear and could be significantly lower than for plasma in synthetic air operated at power level 45 W (twice as high as for oxygen).

Figure 10 shows ozone and NO<sub>2</sub> concentrations as a function of nitrogen content in oxygen fed gas. The concentration of nitrogen varied between 0 and 10%, whereas the total flow of gas was constant at 5 slm. The total power in plasma was 17 W. The concentration of ozone for oxygen gas flow at 5 slm without any nitrogen was approximately 3900 ppm and correlates well with Fig. 7. The increase in nitrogen from 0 to 0.75% had only a minor effect and led to no change in ozone concentration, remaining at approx. 3900 ppm. A small increase in nitrogen concentration between 0.75 and 2.1% had a significant effect on ozone concentration, which increased to approx. 4200 ppm, which is about an 8% rise compared with pure O<sub>2</sub>. Further increase of nitrogen concentration in admixtures ranging from 1 to 10% led to a linear decrease in ozone concentration.

**Fig. 9** O<sub>3</sub> concentration [ppm] in oxygen at various flows ranging from 1.9 to 10 slm



**Fig. 10**  $O_3$  and  $NO_2$  concentration as a function of nitrogen content in oxygen feed gas ranging from 0 to 10%



The fact that small quantities of  $N_2$  improve ozone generation efficiency in DBD micro-discharges had already been observed. For example, Yuan et al. [38] reported that an increase of ozone production can be obtained with 0.3–2%  $N_2$  admixture in  $O_2$ , in a wide range of SIE (100–800 J/l). At 100 J/l, the yield of ozone production increased from 158 g/kWh in pure oxygen to 201.6 g/kWh at  $N_2$  content of 1%. This increase is attributed to an alternative mechanism of  $O(^4S)$  production through  $O_2$  dissociation mediated by electronically excited states of  $N_2$ . The lowest excited triplet state of molecular nitrogen  $N_2(A^3\Sigma_u^+, v)$  is efficiently quenched by  $O_2$ , producing two oxygen atoms [39]. The DBD micro-discharges in  $N_2$ – $O_2$  mixtures populate efficiently the  $v=2$ –5 vibronic levels of the  $N_2(A^3\Sigma_u^+)$  metastable state by direct electron-impact excitation [40]. During the decay of the micro-discharge filament, the  $N_2(A^3\Sigma_u^+)$  metastables are quenched within hundreds of nanoseconds producing additional atomic oxygen, which further reacts mainly with  $O_2$  (provided there is a low content of  $N_2$ ) boosting production of  $O_3$ . With an increasing content of  $N_2$  in the  $N_2$ – $O_2$  mixture, atomic oxygen starts to be consumed in catalytic cycles with the participation of nitrogen oxides, leading to the consumption of both O and  $O_3$ , boosting the production of  $N_xO_y$ . That is why, starting from certain  $N_2$  concentrations in the mixture, the ozone yield at given SIE starts to decrease towards values which are typical for ozone yield in the air. In our case, we observed a peak ozone concentration for  $N_2$  content of 1% with the corresponding  $O_3$  yield of 160 g/kWh at SIE of 56 J/l, which means an approximately 10% increase in ozone concentration with respect to the pure oxygen case.

The results presented in Fig. 10 confirm that the formation of oxygen atoms, essential for  $O_3$  production, was not influenced by  $N_2$  for low admixtures of nitrogen (<0.75%). This very likely means that the EEDF does not significantly change to modify major source of oxygen atoms, i.e. dissociation of the ground-state  $O_2$  molecule (either by the direct electron impact or through kinetic processes enabled by excited  $N_2$ ).

With increasing amount of nitrogen in the mixture (>0.75%), additional reactions between  $N_2$  molecules (excited and metastables) and oxygen molecules influence positively production of atomic oxygen [41]. With a further increase of nitrogen in the mixture (>2%), the EEDF is very likely influenced by inelastic losses of electrons due to the vibrational excitation of the ground electronic state of  $N_2$ . Considering that in the case

of molecular nitrogen, the electron-vibration cross-sections are particularly high [34], the decrease of the EEDF in the energy range which is important for the direct electron-impact dissociation of  $O_2$  (around 5 eV) is quite a plausible scenario. Figure 10 also shows the development of  $NO_2$  concentration as a function of the nitrogen/oxygen ratio. As expected, the  $NO_2$  increase, caused by an increase of  $N_2$ , leads to higher production of atomic nitrogen that reacts with  $O_3$  and creates  $NO_x$ , as described by reaction (4).

Table 1 shows ozone concentration, production, energy efficiency, production yield, and energy cost for selected conditions of ozone generation in synthetic air and oxygen. For synthetic air, the most efficient flow of 2.25 slm led to  $O_3$  concentration of 3690 ppm, which corresponds to the production rate of 1.07 g/h and energy efficiency of 42.21 Wh/g. An increase in the synthetic air flow to 10 slm decreased the concentration to 1878 ppm. On the other hand, the  $O_3$  production increased to 2.41 g/h, and energy efficiency was improved reaching 18.66 Wh/g.

Interestingly, comparison of ozone generation in synthetic air at 45 W and 17 W revealed  $O_3$  productions of 1.07 g/h and 0.79 g/h, respectively. Thus, a 60% decrease of power from 45 to 17 W led to only a 25% decrease in  $O_3$  production. Energy efficiency was improved from 42.21 to 21.51 Wh/g; production yield increased from 24 to 46.5 g/kWh, and energy cost decreased from 92.4 to 38.5 eV/molecule.

The highest values of  $O_3$  concentration and production were reached for oxygen plasma at flow of 1.9 slm and power of 17 W. The  $O_3$  concentration was 9600 ppm, which is near the detection limit (10,000 ppm), and production was 2.34 g/h. An increase in oxygen flow to 10 slm led to an increase in production, which reached 2.77 g/h for 10 slm. The energy efficiency of  $O_3$  production in pure oxygen at 10 slm was found at 6.14 Wh/h, corresponding to a production yield of 163 g/kWh and an energy cost of 11 eV/molecule (which was the smallest energy cost experimentally determined in this work).

The extrapolated values of ozone concentration for oxygen plasma at 17 W showed ozone concentration at 12,181 ppm, which represents production of 2.35 g/h, energy efficiency of 7.25 Wh/g, production yield of 138 g/kWh, and energy cost of 13.0 eV/molecule.

**Table 1** Production and energy efficiency of  $O_3$  generation for selected parameters

Parameters	Concentration [ppm]	Production [g/h]	Energy efficiency [Wh/g]	Production yield [g/kWh]	Energy cost [eV/molecule]
Synth. Air (45 W) 2.25 slm	3690	1.07	42.21	24	92.4
Synth. Air (45 W) 10 slm	1878	2.41	18.66	54	40.9
Synth. Air (17 W) 2.25 slm	2736	0.79	21.51	46.5	38.5
Oxygen (17 W) 1.9 slm	9600	2.34	7.26	138	13.0
Oxygen (17 W) 2.25 slm	8147	2.35	7.22	138	12.9
Oxygen (17 W) 5 slm	3777	2.42	7.01	142	12.5
Oxygen (17 W) 10 slm	2158	2.77	6.14	163	11.0
1% $N_2$ in $O_2$ (17 W) 5 slm	4238	2.72	6.25	160	11.2
Oxygen (17 W) 1.5 slm extrapol	12,181	2.35	7.25	138	13.0

The plasma generated in pure oxygen at a lower power level of 17 W showed the best efficiency of ozone generation from an absolute concentration and production standpoint, but also from the energy efficiency point of view.

Admixtures of a small amount of nitrogen (up to 1%) at a constant flow of 5 slm had a significant effect on ozone generation. The production increased from 2.42 g/h for pure oxygen to 2.72 g/h for 1% nitrogen in oxygen.

The highest production rate with the best energy efficiency was found for oxygen plasma at 10 slm and for 1% nitrogen in oxygen at 5 slm. We conclude that admixture of a small amount of nitrogen into oxygen significantly improves the ozone production, allowing reduction of the working gas ( $O_2$ ) flow in the system and, therefore, also the overall cost of the process, whereas the production and energy efficiency remains roughly at the same level.

## Conclusions

The coplanar DBD system powered by sinusoidal 19 kHz AC high voltage and equipped with a simple passive cooling system was investigated for the ozone generation characteristics and for temperatures established in the thin dielectric surface–plasma layer interface. The passive cooling of the coplanar electrode system in conjunction with the flow of the working gas led to lower ceramic temperatures of about 50 °C, which allows a brief exposure of heat-sensitive biological materials, such as seeds and cereal grains, without affecting their viability negatively.

The first study of ozone generation efficiency by the coplanar DBD system considering all energy inputs (including energy consumed for passive cooling of the reactor) has been performed. The efficiency of ozone production reaches high values of about 50 g/kWh (SIE=75 J/l) and 160 g/kWh (SIE=29 J/l) during continuous AC operation, which exceeds the typical performance of standard surface DBD systems with exposed metallic electrodes (10–15% at similar SIE). Further improvements in ozone generation efficiency might be obtained by employing amplitude-modulation of the driving AC voltage that would lead to a further decrease of the temperature of the gas–dielectric interface. The performance of this passively cooled reactor evidences the applicability of coplanar DBD for the contact treatment of thermally-sensitive surfaces for which a high concentration of ozone is required.

**Acknowledgements** This research was supported by project ref CZ.1.05/2.1.00/03.0086, funded by the European Regional Development Fund; Project LO1411 (NPU I), funded by the Ministry of Education, Youth and Sports of the Czech Republic. B.P. and M.S. were supported by the Czech Science Foundation (Contract No. GA15-04023S).

## References

1. Nassour K, Brahami M, Nemnich S, Hammadi N, Zouzou N, Tilmatine A (2016) Comparative experimental study between surface and volume DBD ozone generator. *Ozone-Sci Eng* 38:70–76. <https://doi.org/10.1080/01919512.2015.1095632>
2. Šimek M, Prukner V, Schmidt J (2011) Optical and electrical characteristics of a single surface DBD micro-discharge produced in atmospheric-pressure nitrogen and synthetic air. *Plasma Sour Sci Technol* 20:025009. <https://doi.org/10.1088/0963-0252/20/2/025009>

3. Šimek M, Ambrico PF, Prukner V (2011) ICCD microscopic imaging of a single micro-discharge in surface coplanar DBD geometry: determination of the luminous diameter of N<sub>2</sub> and Ar streamers. *Plasma Sour Sci Technol* 20:025010. <https://doi.org/10.1088/0963-0252/20/2/025010>
4. Šimek M, Pekárek S, Prukner V (2012) Ozone production using a power modulated surface dielectric barrier discharge in dry synthetic air. *Plasma Chem Plasma Process* 32:743–754. <https://doi.org/10.1007/s11090-012-9382-z>
5. Siemens W (1857) Ueber die elektrostatische induction und die verzögerung des stroms in flaschen-drähten. *Ann der Phys und Chemie* 178:66–122. <https://doi.org/10.1002/andp.18571780905>
6. Kogelschatz U (2003) Dielectric-barrier discharges: their history, discharge physics, and industrial applications. *Plasma Chem Plasma Process* 23:1–46. <https://doi.org/10.1023/A:1022470901385>
7. Pietsch GJ, Gibalov VI (1998) Dielectric barrier discharges and ozone synthesis. *Pure Appl Chem* 70:1169–1174. <https://doi.org/10.1351/pac199870061169>
8. Gibalov VI, Pietsch GJ (2000) The development of dielectric barrier discharges in gas gaps and on surfaces. *J Phys D Appl Phys* 33:2618–2636. <https://doi.org/10.1088/0022-3727/33/20/315>
9. Čech J, Bonaventura Z, Stáhel P, Zemánek M, Dvořáková H, Černák M (2017) Wide-pressure-range coplanar dielectric barrier discharge: operational characterisation of a versatile plasma source. *Phys Plasmas* 24:013504. <https://doi.org/10.1063/1.4973442>
10. Homola T, Krumpolec R, Zemánek M, Kelar J, Synek P, Hoder T, Černák M (2017) An array of micro-hollow surface dielectric barrier discharges for large-area atmospheric-pressure surface treatments. *Plasma Chem Plasma Process* 37:1149–1163. <https://doi.org/10.1007/s11090-017-9792-z>
11. Šimek M, Pekárek S, Prukner V (2010) Influence of power modulation on ozone production using an AC surface dielectric barrier discharge in oxygen. *Plasma Chem Plasma Process* 30:607–617. <https://doi.org/10.1007/s11090-010-9245-4>
12. Zhang YF, Wei LS, Liang X, Deng HZ, Šimek M (2018) Characteristics of the discharge and ozone generation in oxygen-fed coaxial DBD using an amplitude-modulated AC power supply. *Plasma Chem Plasma Process* 38:1199–1208. <https://doi.org/10.1007/s11090-018-9922-2>
13. Kováčik D (2006) Surface modification of polymer materials by atmospheric-pressure plasma induced grafting. Comenius University, Slovakia
14. Černák M, Kováčik D, Ráhel' J, Stáhel P, Zahoranová A, Kubincová J, Tóth A, Černáková L (2011) Generation of a high-density highly non-equilibrium air plasma for high-speed large-area flat surface processing. *Plasma Phys Control Fusion* 53:124031. <https://doi.org/10.1088/0741-3335/53/12/124031>
15. Skácelová D, Danilov V, Schäfer J, Quade A, Stáhel P, Černák M, Meichsner J (2013) Room temperature plasma oxidation in DCSBD: a new method for preparation of silicon dioxide films at atmospheric pressure. *Mater Sci Eng, B* 178:651–655. <https://doi.org/10.1016/j.mseb.2012.10.017>
16. Skácelová D, Sládek P, Stáhel P, Pawera L, Haničinec M, Meichsner J, Černák M (2014) Properties of atmospheric pressure plasma oxidized layers on silicon wafers. *Open Chem* 13:376–381. <https://doi.org/10.1515/chem-2015-0047>
17. Medvecká V, Kováčik D, Zahoranová A, Stupavská M, Černák M (2016) Atmospheric pressure plasma assisted calcination of organometallic fibers. *Mater Lett* 162:79–82. <https://doi.org/10.1016/j.matlet.2015.09.109>
18. Medvecká V, Kováčik D, Zahoranová A, Černák M (2018) Atmospheric pressure plasma assisted calcination by the preparation of TiO<sub>2</sub> fibers in submicron scale. *Appl Surf Sci* 428:609–615. <https://doi.org/10.1016/j.apsusc.2017.09.178>
19. Prysiazhnyi V, Brablec A, Čech J, Stupavská M, Černák M (2014) Generation of large-area highly-non-equilibrium plasma in pure hydrogen at atmospheric pressure. *Contrib Plasma Phys* 54:138–144. <https://doi.org/10.1002/ctpp.201310060>
20. Krumpolec R, Čech J, Jurmanová J, Ďurina P, Černák M (2017) Atmospheric pressure plasma etching of silicon dioxide using diffuse coplanar surface barrier discharge generated in pure hydrogen. *Surf Coat Technol* 309:301–308. <https://doi.org/10.1016/j.surfcoat.2016.11.036>
21. Homola T, Shekargoftar M, Dzik P, Krumpolec R, Ďurašová Z, Veselý M, Černák M (2017) Low-temperature (70°C) ambient air plasma-fabrication of inkjet-printed mesoporous TiO<sub>2</sub> flexible photoanodes. *Flex Print Electron* 2:035010. <https://doi.org/10.1088/2058-8585/aa88e6>
22. Homola T, Pospíšil J, Krumpolec R, Souček P, Dzik P, Weiter M, Černák M (2018) Atmospheric dry hydrogen plasma reduction of inkjet-printed flexible graphene oxide surfaces. *ChemSusChem* 11:941–947. <https://doi.org/10.1002/cssc.201702139>
23. Homola T, Dzik P, Veselý M, Kelar J, Černák M, Weiter M (2016) Fast and low-temperature (70°C) mineralization of inkjet printed mesoporous TiO<sub>2</sub> photoanodes using ambient air plasma. *ACS Appl Mater Interfaces* 8:33562–33571. <https://doi.org/10.1021/acsami.6b09556>
24. Weltmann KD, Kolb JF, Holub M et al (2019) The future for plasma science and technology. *Plasma Process Polym* 16:1–29. <https://doi.org/10.1002/ppap.201800118>

25. Puač N, Gherardi M, Shiratani M (2018) Plasma agriculture: a rapidly emerging field. *Plasma Process Polym* 15:1700174. <https://doi.org/10.1002/ppap.201700174>
26. Mošovská S, Medvecká V, Halászová N, Ďurina P, Valík E, Mikulajová A, Zahoranová A (2018) Cold atmospheric pressure ambient air plasma inhibition of pathogenic bacteria on the surface of black pepper. *Food Res Int* 106:862–869. <https://doi.org/10.1016/j.FOODRES.2018.01.066>
27. Stolárik T, Henselová M, Martinka M, Novák O, Zahoranová A, Černák M (2015) Effect of low-temperature plasma on the structure of seeds, growth and metabolism of endogenous phytohormones in pea (*Pisum sativum* L.). *Plasma Chem Plasma Process* 35:659–676. <https://doi.org/10.1007/s11090-015-9627-8>
28. Zahoranová A, Hoppanová L, Šimončicová J, Tučeková Z, Medvecká V, Hudecová D, Kaliňáková B, Kováčik D, Černák M (2018) Effect of cold atmospheric pressure plasma on maize seeds: enhancement of seedlings growth and surface microorganisms inactivation. *Plasma Chem Plasma Process* 38:969–988. <https://doi.org/10.1007/s11090-018-9913-3>
29. Waskow A, Betschart J, Butscher D, Oberbossel G, Klöti D, Büttner-Mainik A, Adamcik J, Rudolf von Rohr P, Schuppler M (2018) Characterization of efficiency and mechanisms of cold atmospheric pressure plasma decontamination of seeds for sprout production. *Front Microbiol* 9:3164. <https://doi.org/10.3389/FMICB.2018.03164>
30. Brandenburg R, Bongers W, Reuter S et al (2018) White paper on the future of plasma science in environment, for gas conversion and agriculture. *Plasma Process Polym* 16:1700238. <https://doi.org/10.1002/ppap.201700238>
31. Ambrico PF, Šimek M, Morano M, De Miccolis Angelini RM, Minafra A, Trotti P, Ambrico M, Prukner V, Faretra F (2017) Reduction of microbial contamination and improvement of germination of sweet basil (*Ocimum basilicum* L.) seeds via surface dielectric barrier discharge. *J Phys D Appl Phys* 50:305401. <https://doi.org/10.1088/1361-6463/aa77c8>
32. Mohammad Z, Kalbasi-Ashtari A, Riskowski G, Castillo A (2019) Reduction of salmonella and shiga toxin-producing escherichia coli on alfalfa seeds and sprouts using an ozone generating system. *Int J Food Microbiol* 289:57–63. <https://doi.org/10.1016/j.IJFOODMICRO.2018.08.023>
33. Pawlat J, Starek A, Sujak A, Terebun P, Kwiatkowski M, Budzeń M, Andrejko D (2018) Effects of atmospheric pressure plasma jet operating with DBD on *Lavatera thuringiaca* L. seeds' germination. *PLoS ONE* 13:e0194349. <https://doi.org/10.1371/journal.pone.0194349>
34. Šimek M (2014) Optical diagnostics of streamer discharges in atmospheric gases. *J Phys D Appl Phys* 47:463001. <https://doi.org/10.1088/0022-3727/47/46/463001>
35. Jōgi I, Erme K, Levoll E, Stamate E (2017) Radical production efficiency and electrical characteristics of a coplanar barrier discharge built by multilayer ceramic technology. *J Phys D Appl Phys* 50:465201. <https://doi.org/10.1088/1361-6463/aa8dab>
36. Parra-Rojas FC, Passas M, Carrasco E, Luque A, Tanarro I, Simek M, Gordillo-Vázquez FJ (2013) Spectroscopic diagnostics of laboratory air plasmas as a benchmark for spectral rotational (gas) temperature determination in TLEs. *J Geophys Res Sp Phys* 118:4649–4661. <https://doi.org/10.1002/jgra.50433>
37. Machala Z, Janda M, Hensel K, Jedlovský I, Leštinská L, Foltin V, Martišoviš V, Morvová M (2007) Emission spectroscopy of atmospheric pressure plasmas for bio-medical and environmental applications. *J Mol Spectrosc* 243:194–201. <https://doi.org/10.1016/j.jms.2007.03.001>
38. Yuan D, Xie S, Ding C, Lin F, He Y, Wang Z, Cen K (2018) The benefits of small quantities of nitrogen in the oxygen feed to ozone generators. *Ozone Sci Eng* 40:313–320. <https://doi.org/10.1080/01919512.2018.1427553>
39. Kossyi IA, Kostinsky AY, Matveyev AA, Silakov VP (1992) Kinetic scheme of the non-equilibrium discharge in nitrogen-oxygen mixtures. *Plasma Sour Sci Technol* 1:207–220. <https://doi.org/10.1088/0963-0252/1/3/011>
40. Šimek M, Ambrico PF, Prukner V (2017) Evolution of  $N_2(A^3\Sigma_u^+)$  in streamer discharges: influence of oxygen admixtures on formation of low vibrational levels. *J Phys D Appl Phys* 50:504002. <https://doi.org/10.1088/1361-6463/aa96f3>
41. Šimek M, Bonaventura Z (2018) Non-equilibrium kinetics of the ground and excited states in  $N_2-O_2$  under nanosecond discharge conditions: extended scheme and comparison with available experimental observations. *J Phys D Appl Phys* 51:504004. <https://doi.org/10.1088/1361-6463/aadcd1>